

A Novel Threshold Accelerometer With Postbuckling Structures for Airbag Restraint Systems

Jian Zhao, Jianyuan Jia, Hongxi Wang, and Wanli Li

Abstract—Based on the postbuckling theory of large deflection beams, the nonlinear stiffness of a postbuckling beam is deduced and in agreement with the results of buckling experiments. Then, a novel postmachined threshold accelerometer is designed, which consists of eight oblique postbeams with an inertial mass in the middle to ensure its single moving direction and an electrical contact part fabricated on the bottom of the inertial mass. The threshold accelerometer is an integration of a threshold sensor and an inertial driven actuator used in airbag restraint systems. When the acceleration reaches the threshold, the beams buckle and close the threshold accelerometer, and when it gets down to be a certain value, the accelerometer opens quickly under the effect of the elastic force developed by the postbuckling beams. Compared with the design models of other threshold accelerometers with linear beam structures, the nonlinear postbuckling beams are introduced as threshold sensing elements. A number of design factors such as the air film damping and the contact force are taken into full consideration, thus establishing the dynamic equation of the accelerometer under coupled forces. The dynamical simulation for the strong nonlinear system with elliptic integrals indicates its good threshold characteristic and high contact reliability. The threshold accelerometer responds within 4 ms when it is triggered by a threshold acceleration $a_c = 20$ g, and cuts off quickly when the cutoff acceleration is under $a_d = 5$ g. Meanwhile, the unstable contact time is only 0.02 ms for the contact force to reach 50 mN, which guarantees the contact resistance to be less than 20 m Ω . With the results of the dynamic simulation, supported by previous buckling experiments, the accelerometer can provide accurate threshold sensing without false actuations under interferences outside, especially electromagnetic and vibration interferences, and hence their wide applications in safe-arming systems.

Index Terms—Microelectromechanical systems (MEMS), nonlinear stiffness, postbuckling, threshold accelerometer.

I. INTRODUCTION

MOST accidents occur due to the malfunction of airbag restraint systems under interferences such as electromagnetic and pulse noises. As a result, modern inertial measuring and controlling systems including vibration isola-

tion systems, systems in aircrafts and airbag restraint systems require threshold accelerometers not only to have the characteristics of fast response, high sensitivity, low cost and good reliability but also to resist any outside disturbances. Among these accelerometers, since it needs to sense the threshold acceleration and switch the circuit between On and Off states depending on the acceleration amplitude, the threshold accelerometer with postbuckling beams is an integration of a threshold sensor and an inertial driven actuator. The inertial force used to actuate the accelerometer and supply a stable contact force when the circuit is switched on is different from the electrostatic force and electrothermal force widely used in microactuators. When the outside acceleration is less than a certain value, the threshold accelerometer can switch off the circuit automatically. Therefore, with its perfect antijamming capability on electromagnetic and vibration interferences, the mechanical threshold accelerometer is an excellent device in airbag restraint systems in automobiles or other safe-arming systems.

Bistable postbuckling mechanisms which possess excellent performance in decreasing power consumption are very useful in the design of a wide variety of microdevices. The performance of the threshold accelerometer depends largely on the design of the threshold sensing element. Fortunately, the nonlinear postbuckling bent-beam structure can fulfill the requirements of the static design of the threshold accelerometer. As is known, the bistability and the nonlinear stiffness occur when a vertical force is applied to the middle of the bent-beam. Taking advantage of the bistability of the bent-beam, several kinds of bistable microactuators have been fabricated and applied as the subsystems in various microelectromechanical systems (MEMS) fields. For example, Wilcox *et al.* [1] design an on-chip microactuator with the linear compliant tensural bistable mechanisms. Enikov *et al.* [2] design a V-shaped thermal microactuator with buckling beams. However, the precise computation model for the buckling beam based on the large deflection theory has not been built. In [3], a linear postfeeding system with compliant bistable mechanisms is designed. Hwang *et al.* [4] also use the equivalent stiffness model of buckling structures to design a chevron-type bistable microactuator. Receveur *et al.* [5] design a bistable DC switch for biomedical application with a double-clamped beam structure. However, these postbuckling bent beams with good threshold characteristics have not yet been applied in designing threshold accelerometers. In contrast, other MEMS structures, such as cantilever and residual stress buckled beams, are used as sensing elements in acceleration threshold switches in the inertial systems [6]. Go *et al.* [7] design a snapping microswitch with a prestressed buckled beam

Manuscript received September 9, 2006; revised February 5, 2007; accepted February 5, 2007. This work was supported in part by the National Nature Science Foundation and in part by the Academy of Engineering Physics under Grant 10476019. The associate editor coordinating the review of this paper and approving it for publication was Dr. John Vig.

J. Zhao, J. Jia, and H. Wang are with the College of Electro-Mechanical Engineering, Xidian University, Xi'an, Shaanxi 710071, China (e-mail: zhaojian0403@163.com; jyjia@xidian.edu.cn; whx_yz@163.com).

W. Li is with the Department of Foreign Language, Xi'an University of Science and Technology, Xi'an, Shaanxi 710054 China (e-mail: liwanli68@126.com).

Color versions of one or more of the figures in this paper are available online at <http://ieeexplore.ieee.org>.

Digital Object Identifier 10.1109/JSEN.2007.897936

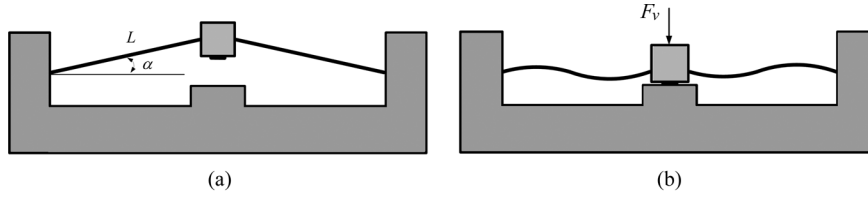


Fig. 1. Bent-beam structure. (a) Original state. (b) Postbuckling state.

which is actuated by the electrostatic force. Matsunaga *et al.* [8] use the squeeze film effect to extend the holding time of the acceleration switch for the side airbag system. However, the linear beam structure used in this acceleration switch has no obvious threshold characteristic and is not an excellent design element in threshold switch. Michaelis *et al.* [9] and Wycisk *et al.* [10] design a new type of acceleration threshold sensor on the top of a CMOS signal processing circuit. Selvakumar *et al.* [11] use cantilever structures to design an array of threshold accelerometers for a wide range of threshold acceleration sensing systems. In addition, Sulfridge *et al.* [12] analyze the nonlinear dynamic characteristics of a tunable postmechanical bistable system with buckled beams, and point out the potential applications of buckled beams in switching. Although the compressed bistable buckled beams are really excellent structures, the dimension consistency of the residual-compressive-stress beams in the MEMS bulk production cannot be easily achieved. Consequently, postbuckling bent beams are considered in designing threshold accelerometers. Due to the strong nonlinearity of the postbuckling beam, the dynamics of the bent-beam system is also nonlinear. Besides the nonlinear stiffness, the influences of the damping force and contact force on the dynamics of a threshold accelerometer should also be taken into full consideration to improve the accelerometer's overall performance.

In this paper, the nonlinear stiffness of the postbuckling bent-beam is analyzed in details according to the large deflection buckling theory. The results of the stiffness analysis are in good accordance with those of experiments. Based on the precise stiffness analysis, a novel threshold accelerometer with oblique supported beams is designed, which consists of eight oblique postbeams with a mass in the middle. The symmetry of the structure ensures the inertial mass to move in a single direction. The dynamic design model of the accelerometer under coupled forces is established. Different from other design models, the film damping effects and the contact resistance are also considered as important factors in the design method proposed. Meanwhile, the contact stability and antijamming capability of the sensing system are investigated.

II. ANALYSIS AND DESIGN OF THE INERTIAL DEVICE

A. Stiffness Analysis of the Bent-Beam Structure

Bent-beam structures have distinct advantages over the other commonly used folded-beam ones since the former can provide a nonlinear vertical motion and threshold structure buckling. Furthermore, potential applications are developed in designing microactuators and optical switches.

To solve the postbuckling problems of small deformation beams, the predominant approach is used as a nonlinear finite-element (FE) model, or to resort to a linear analytical

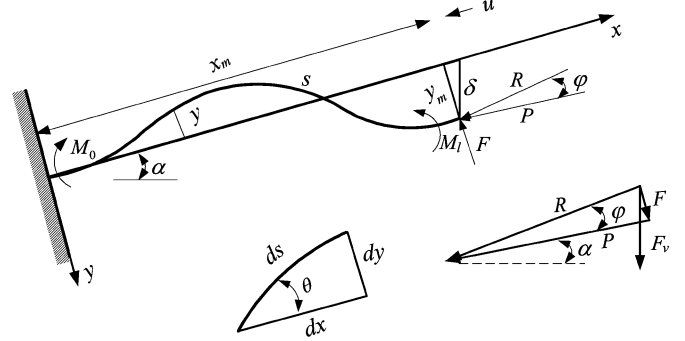


Fig. 2. Deformation of postbuckling bent-beam under combined load.

model based on the small deflection theory, which only agrees with experiments in a relatively limited range of loadings. The apex displacement of the bent-beam can only be reduced in almost linear proportion to the vertical force in the design process of microactuators [13], [14], and the error is large compared with the results of experiments. This lack of a simple and yet accurate tool for analyzing the postbuckling bent beams results in a poor initial “guess” of the desired geometry and multidesign iterations, thus not being able to provide an insight into the deformation problems. Thus, the large-deflection-buckling theory is needed to solve the intractability of the geometric nonlinear control equations of the bent-beam to establish an accurate design model of the threshold accelerometer.

A typical bent-beam structure is shown in Fig. 1. The constraint beam is subjected to both compression and lateral bending moments, thus resulting in vertical displacement. Based on the symmetry of the structure, the left half span of the bent-beam with reaction forces is analyzed and the coordinated system used is shown in Fig. 2.

Using the geometric symmetry, force and moment equilibrium conditions, the geometrical relations (1) at the ending point and the moment (2) at any section of the bent-beam can be expressed as

$$y_m = \delta \cos \alpha, x_m = L - u = L - \delta \sin \alpha \quad (1)$$

$$M = -R(y + y_m) \cos \varphi - R(x_m - x) \sin \varphi + M_l \quad (2)$$

where δ represents the displacement of the fixed ending point, α the initial angle of the beam, L the length, (x_m, y_m) the coordinate values of the ending point, φ the obliquity of elastic force R , and θ the angle of any section along the beam. M_0 and M_l stand for the bending moments at the left and right clamped edges, respectively. P and F , which can be expressed as $P = R \cos \varphi$ and $F = R \sin \varphi$, are axial and transversal components of force R . F_v is the vertical elastic force. Assuming that the deformed

shape of the beam can be described by a longitudinal displacement $u(x)$ and transversal displacement $y(x)$, the governing equation of the postbuckling of a clamped-clamped supported bent-beam can be given as

$$\begin{cases} \frac{d\theta}{ds} = \frac{-R \cos \varphi (y+y_m) - R \sin \varphi [x_m - x] + M_l}{EI} \\ \frac{dy}{ds} = \sin \theta \\ \frac{dx}{ds} = \cos \theta \end{cases} \quad (3)$$

where E is the Young modulus and I is the moment of inertia.

By applying boundary conditions of the governing equation

$$\begin{cases} \theta(L) = 0, y(L) = -y_m, x(L) = x_m \\ \theta(0) = 0, y(0) = 0, x(0) = 0 \end{cases} \quad (4)$$

conditions in (4) are self-explanatory and (1) indicates that the center of the bent-beam can only move in the vertical direction, as shown in Fig. 1. The above conditions constrain the bent-beam to symmetric buckling modes only, which result in a closed-form solution of the tip displacement and reaction force. Phenomena such as the snap-through, which include transition through asymmetric modes, are not included in the present model.

The differentiation of (3) with respect to s yields

$$\frac{d^2\theta}{ds^2} = -\frac{R}{EI} \cos \varphi \sin \theta + \frac{R}{EI} \sin \varphi \cos \theta. \quad (5)$$

Integrating (5) with respect to θ results in

$$\begin{aligned} \frac{1}{2} \left(\frac{d\theta}{ds} \right)^2 &= \frac{R}{EI} \cos \varphi \cos \theta + \frac{R}{EI} \sin \varphi \sin \theta + c_1 \\ &= \frac{1}{2} \left(\frac{M}{EI} \right)^2. \end{aligned} \quad (6)$$

Taking into the consideration of the bending moment $M = 0$ at the inflexion point where the cross-section angle $\theta = \theta^*$, a relation between ϕ and the ending point displacement x_m, y_m , can be found from (6)

$$c_1 = -\frac{R}{EI} \cos(\theta^* - \varphi). \quad (7)$$

Considering the symmetric buckling modes of the postbuckling beam, the relation between the moments at the two ending points can be found by substituting (4) into (6)

$$M_l = M_0. \quad (8)$$

Substituting (4) and (8) into (2), the relation between ϕ and the ending point displacement x_m, y_m , can be found in terms of

$$\tan \varphi = \frac{F}{P} = \frac{y_m}{x_m}. \quad (9)$$

Then, moment M_l at the ending point can be written as by substituting the boundary conditions (7) into (6)

$$M_l = \sqrt{2REI[\cos(\theta - \varphi) - \cos(\theta^* - \varphi)]}. \quad (10)$$

The moment-curvature equation of the buckled beam can be written from (6) as

$$\frac{d\theta}{ds} = \pm \sqrt{\frac{2R}{EI} \sqrt{\cos(\theta - \varphi) - \cos(\theta^* - \varphi)}}. \quad (11)$$

Then, the constraint condition of invariable length of the beam is obtained by integrating (11) with respect to s

$$L = \sqrt{\frac{2EI}{R}} \int_{-\theta^*}^{\theta^*} \frac{d\theta}{\sqrt{\cos(\theta - \varphi) - \cos(\theta^* - \varphi)}}. \quad (12)$$

The constraint condition of the displacement of the fixed ending point is

$$(L - u) \cos \varphi + y_m \sin \varphi = \int_0^L (\cos \theta \cos \varphi - \sin \theta \sin \varphi) ds. \quad (13)$$

Based on the geometric relations and force equilibrium relationship in Fig. 2, the vertical elastic force F_v can be written as

$$F_v = R(\cos \varphi \sin \alpha + \sin \varphi \cos \alpha) \quad (14)$$

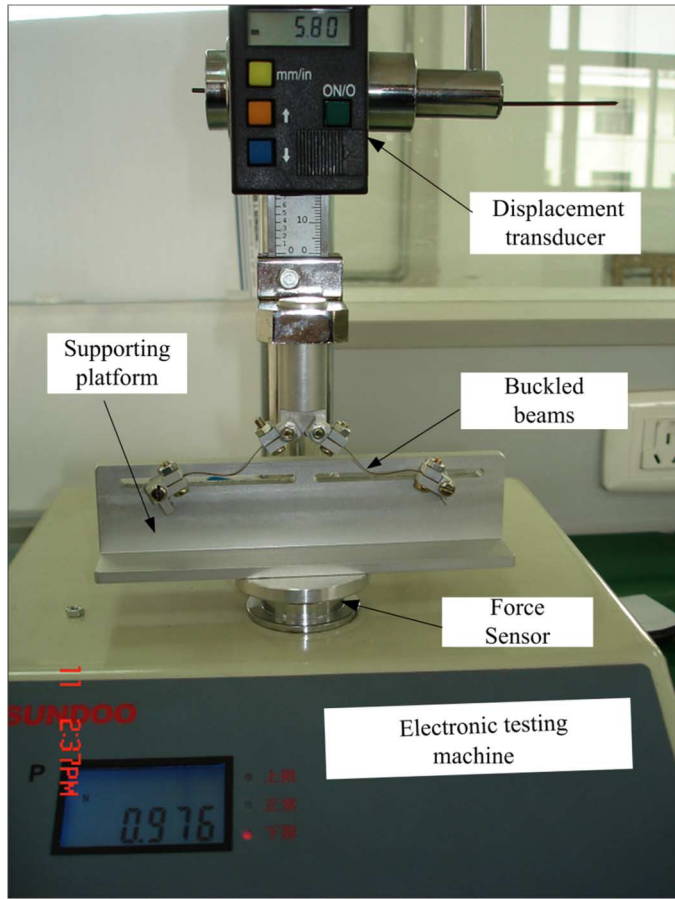
where R and φ are implicit functions of the vertical displacement δ .

Therefore, with a given control parameter δ , the elastic force R and its obliquity ϕ can be determined by solving (9), (12), and (13). Then, the nonlinear stiffness of the postbuckling beam subjected to combined forces can be found by solving (3) with the incremental-displacement numerical method.

For validating the theoretical deduction and the further applications of postbuckling beams, an electronic testing device is designed, as shown in Fig. 3(a), and a run of experiments are conducted to verify the nonlinear stiffness value analytically calculated.

As shown in Fig. 3(a), the postbuckling testing device consists of a displacement transducer, a force sensor, a supporting platform and two output screens. The oblique be-bronze beams are fixed on the postbuckling platform when the vertical force is applied to the fixed middle point. When the middle tip moves, the values of the displacement and the corresponding reaction force can be sensed and displayed on two different screens, respectively. The parameters of the beam structure can be determined, as shown in Table I.

Fig. 3(b) shows the elastic vertical force F_v versus the vertical displacement δ . When the inertial force exceeds the critical buckling force, the elastic force F_v decreases as the vertical displacement δ increases. The force F_v decreases to zero at the unstable equilibrium position, and then the buckled beam snaps to another equilibrium position automatically, which is consistent with the results accomplished by our experiments. By regulating the initial angle and dimensions of the postbuckling beams, different force-displacement curves can be obtained. Therefore, different kinds of threshold acceleration sensing devices can be designed by using the postbuckling nonlinear stiffness and the threshold characteristic of the bent-beam structures.



(a)

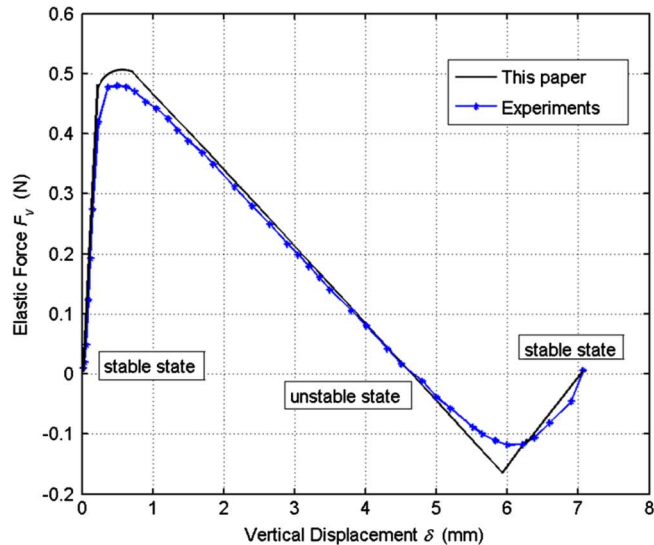


Fig. 3. Testing and simulation of postbuckling beams. (a) Electronic testing device for post buckling beams. (b) Elastic force versus transverse displacement.

B. Structure of the Accelerometer

The postbuckling beams can be used in the design of a threshold accelerometer which can be adapted to switch between On- and Off-states depending upon the amplitude of the acceleration applied to trigger the accelerometer. For example, when the acceleration amplitude exceeds the predicted

TABLE I
STATIC STRUCTURE PARAMETERS OF THE BEAM

Symbol	Value
Initial angle α ($^\circ$)	12
Length L (m)	0.03
Beam width w (m)	0.001
Thickness h (m)	0.2×10^{-3}
Young modulus E (Gpa)	160

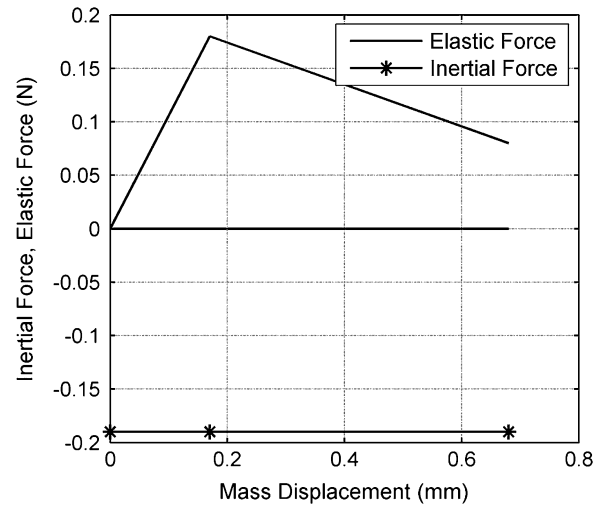


Fig. 4. Static design principle.

threshold a_c , the threshold accelerometer needs to convert the Off-state into the On-state. Then, the circuit controlled by the accelerometer is switched on. On the contrary, when the acceleration amplitude is under the cut-threshold a_d , the accelerometer is shifted to the Off-state rapidly.

The static design principle is shown in Fig. 4. As is known, the driven force of the threshold accelerometer is the inertial force. According to the above analysis of the postbuckling beam, the elastic force decreases as the mass displacement increases, and the elastic force at the contact point should be less than the inertial force. Hence, a certain contact force can be supplied by the difference between the inertial force and the elastic force. When the distance between the inertial mass and the fixed contact is large, the elastic force at the contact point is positive, and when the distance is small, the elastic force is negative and the contact force becomes large. Therefore, the contact force obviously depends on the inertial force and the distance the inertial mass moves.

Based on the above analysis of the postbuckling bent-beam, a novel threshold accelerometer is designed, as shown in Fig. 5. Deep-reactive-ion-etching (DRIE) technology is introduced to manufacture the accelerometer, which allows the fabrication of microstructures with high aspect ratios (etch depth divided by lateral feature size) and near vertical sidewalls ($90^\circ \pm 2^\circ$) in single-crystal or polycrystalline wafers. The gold contact point can be sputtered on the surfaces of the structure. The typical thickness of a double-sided polished 150 mm wafer is $500 \mu\text{m}$,

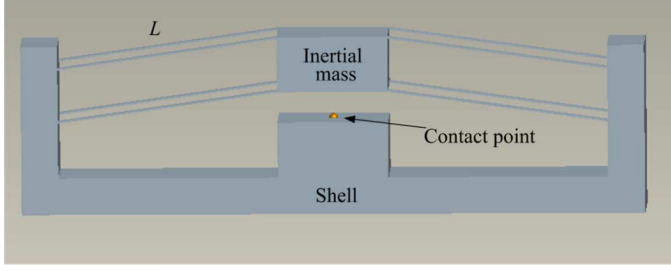


Fig. 5. The threshold accelerometer.

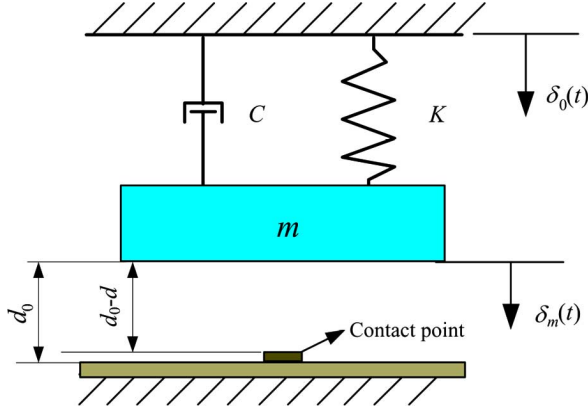


Fig. 6. Motion schematic diagram of the threshold accelerometer.

which requires about 2.5 h for a 100 μm -wide trench. The fabrication processes include one layer of SiO_2 for electrical isolation, two layers of SOI for mechanical structures. By employing the DRIE process, the only work that needs to be done by users is to draw masks and do the postprocessing including etching the sacrificial layers to release the structure layers.

The accelerometer consists of eight oblique beams centrally clamped with an inertial mass, a length of L , and an initial angle α . After the vertical inertial force applied on the mass m reaches the critical value, the bent-beams buckle and push the inertial mass to a predicted position to satisfy the design task. Eight supporting beams are used to prevent the torsion moments. The simplicity of the structure guarantees the bulk production of this kind of accelerometer.

III. DYNAMIC DESIGN AND SIMULATION

Since the dynamic characteristics of a threshold accelerometer depend upon the movement of the inertial mass, the motion characteristic of the inertial mass should be first analyzed. Considering the gas film damping coefficient and the nonlinear contact process, the motion principle of the inertial mass is described, as shown in Fig. 6.

$\delta_0(t)$ represents the movement of the case, $\delta_m(t)$ the movement of the mass, and $\delta(t) = \delta_m(t) - \delta_0(t)$ the relative movement of the mass. Therefore, according to the basic principle of mechanics, the dynamic equation of the accelerometer system can be written as

$$m\ddot{\delta}_m(t) = -K[\delta_m(t) - \delta_0(t)] - C[\dot{\delta}_m(t) - \dot{\delta}_0(t)] - F_d \quad (15)$$

$$K = 8K_1 \quad (16)$$

where K is the total stiffness of eight oblique beams, K_1 the nonlinear stiffness of postbuckling beam, F_d the contact force, C the damping coefficient, and $\dot{\delta}_0$ the acceleration of the case.

Then, substituting $\delta(t) = \delta_m(t) - \delta_0(t)$ into (15), the dynamic equation can be changed as

$$m\ddot{\delta} + C\dot{\delta} + K\delta + F_d = -m\ddot{\delta}_0. \quad (17)$$

Note that $L \times w \times h$ represents the dimension of the beam, $a_m \times b_m \times c_m$ the dimension of the inertial mass, d the height of the contact, and d_0 the distance between the undersurface and the case.

Then, the gas film damping coefficient [15]–[18] can be described as

$$C = \frac{\mu\nu a_m b_m^3}{d_0^3} \quad (18)$$

where μ is the gas kinetic viscosity and $\nu = 1 - 0.6a_m/b_m$ the auxiliary value.

Based on the elastic Hertz theory [19], [20], the relation between the contact force and the displacement can be derived as follows:

$$F_d = \begin{cases} \frac{2E\sqrt{r}[\delta(t) - d_0 + d]^3}{3(1-\sigma^2)}, & \delta > d_0 - d \\ 0, & \delta \leq d_0 - d \end{cases} \quad (19)$$

where E represents Young's modulus, σ the Poisson ratio, and r the contact radius.

Substituting (18), (19), and the nonlinear stiffness K into the control (17), the time response of the accelerometer system can be simulated.

The complicated control system developed in this research is of strong nonlinearity and is hard to be solved analytically. Hence, the Runge–Kutta method is used to simulate its kinetic characteristics.

Based on the static design of the threshold accelerometer and the nonlinear stiffness of the buckled beam, the constraint conditions of dynamic design of the threshold acceleration sensing devices are found as follows.

- The inertial threshold force exceeds the critical buckling load of the oblique beam

$$m \cdot a_c \geq K \cdot \delta_{cr} \quad (20)$$

where a_c is the threshold acceleration, K the total stiffness of the structure, and δ_{cr} the critical buckling position.

- The contact force must be more than 50 mN [20]–[23] to ensure the contact stability

$$F_d = m \cdot a_c - K \cdot d \geq 50 \text{ mN}. \quad (21)$$

- If the acceleration is less than the cut-threshold, the threshold accelerometer cuts off automatically

$$K \cdot d \geq m \cdot a_d \quad (22)$$

where a_d is the cutoff acceleration.

Therefore, with these constraint conditions (20)–(22) of designing the accelerometer and given $a_c = 20 \text{ g}$ and $a_d = 5 \text{ g}$,

TABLE II
 STATIC STRUCTURE PARAMETERS OF THE THRESHOLD ACCELEROMETER

Symbol		Value
Mass	m (Kg)	0.52×10^{-3}
Length	L (m)	1×10^{-3}
Beam width	w (m)	1×10^{-4}
Beam thickness	h (m)	3×10^{-5}
Initial distance	d_0 (m)	7×10^{-5}
Contact height	d (m)	1×10^{-5}
Initial angle	α (°)	8
Contact radius	r (m)	1.2×10^{-4}

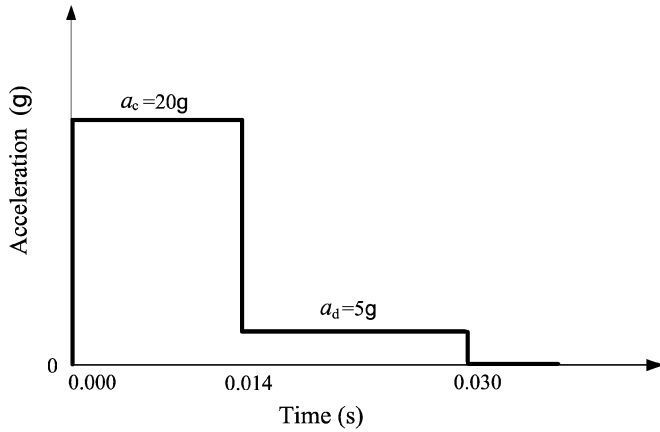


Fig. 7. Step-up acceleration signal.

we can determine the structure parameters by using the linear search method [Table II].

Different from relays, the threshold accelerometer depending on the acceleration amplitude needs to switch between On- and Off-states. Hence, the threshold accelerometer is an integration of a sensor and an actuator. Therefore, we can use a step-up acceleration signal shown in Fig. 7, to simulate the dynamic characteristics of the microaccelerometer to validate the design and analysis theory of the threshold accelerometer.

Figs. 8 and 9 show the dynamic responses of the threshold accelerometer applied to several accelerations with different amplitudes, where a is the outside acceleration applied on the accelerometer. For $a < a_c$, the threshold accelerometer never switches and the contact force keeps zero, which indicates that the threshold accelerometer remains on the Off-state. For $a = a_c$, it only takes 4.0 ms for the accelerometer to convert from Off-state to On-state, and the unstable contact time is 0.02 ms which can reduce the influence of the contact heat and the electric arc effectively. Meanwhile, the contact force is larger than 50 mN which can decrease the contact resistance and improve the contact stability. When the acceleration amplitude is under the cut-threshold ($a = a_d$), the accelerometer cuts off rapidly. In Fig. 9, when the accelerometer is triggered by the threshold acceleration, the contact force can be kept in a certain value to switch on the circuit with a low contact resistance until the acceleration is less than the cut-threshold. For $a > a_c$, the response

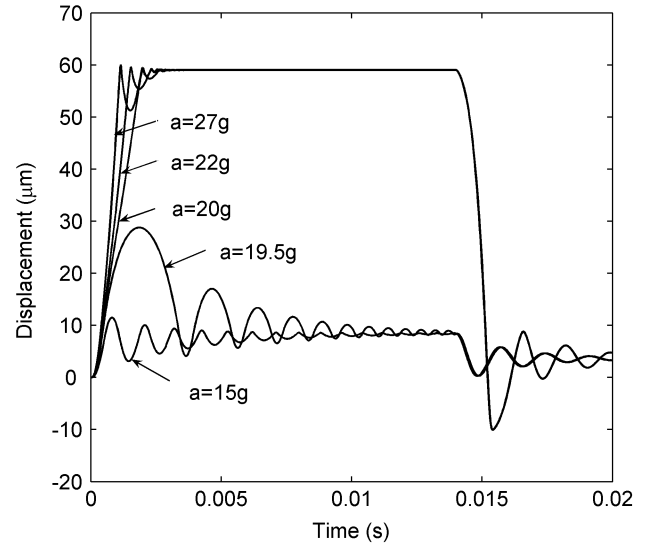


Fig. 8. Time response of the accelerometer for different accelerations.

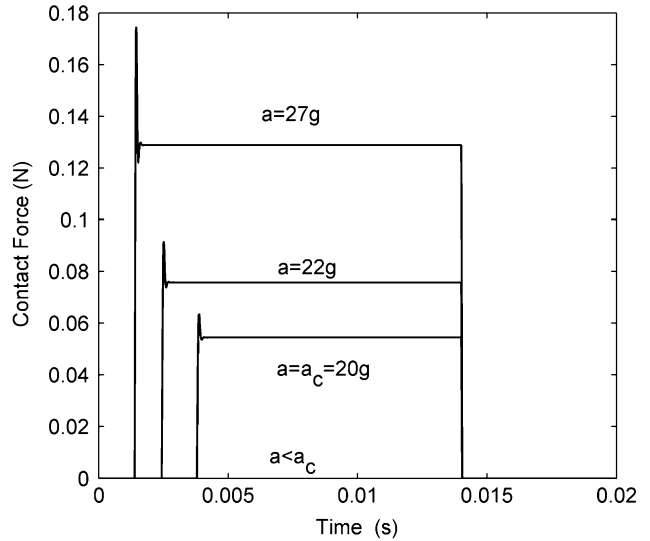


Fig. 9. Contact forces of the threshold accelerometer for different accelerations.

time decreases and the contact force increases as the acceleration amplitude increases. The curves in Fig. 8 also show that the system stays at an overdamped state and we can regulate the gas film damping coefficient to reduce the response time, correspondingly weakening the antijamming capability of the system.

IV. ANTIJAMMING PERFORMANCE

In this section, the dynamic response of the threshold accelerometer under the interference noises is analyzed by using the numerical simulation. Then, the amplitudes of different noisy signals that the system can bear are obtained by the dynamic simulation. For pulse noise, a_i represents the largest amplitude that the threshold accelerometer can resist at a definite pulsewidth t . For harmonic noises, due to the difficulty in confirming the effective frequency of the mixed harmonic noises, the sinusoidal signal is introduced as the interference

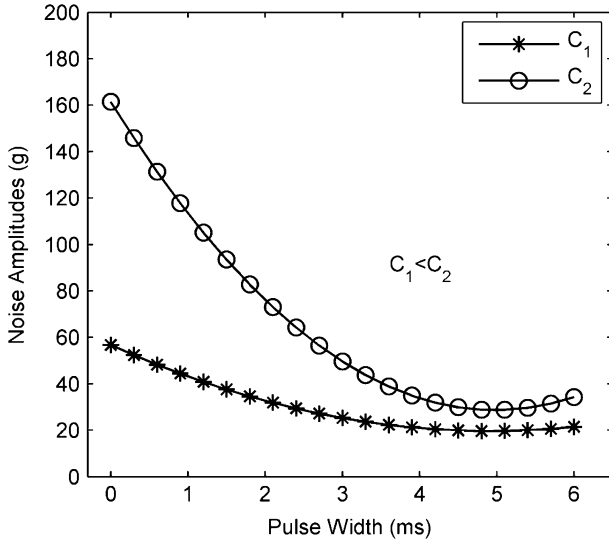


Fig. 10. Amplitudes that the system can bear versus pulse widths.

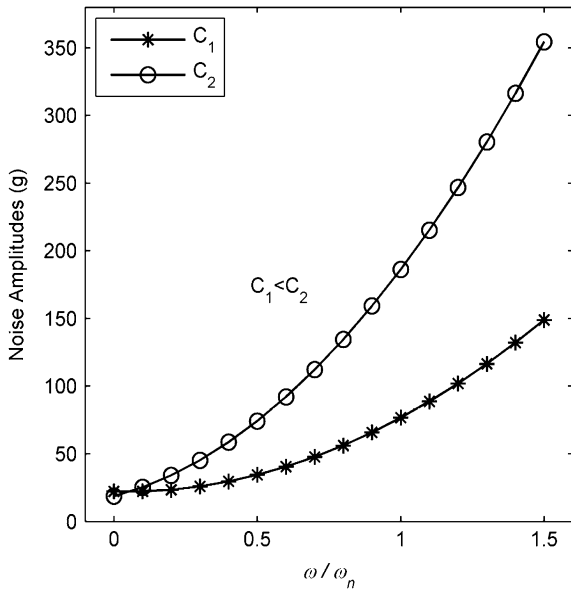


Fig. 11. Noise amplitudes that the system can bear with different frequencies.

in the antijamming capability simulation. While sinusoidal interfering signals with different frequencies are applied, the antijamming performance can be expressed by the largest amplitude a_i that the system can bear.

Since the nonlinearity of the threshold accelerometer structure, the natural frequency ω_n is obtained by simulating the system response numerically. The procedure above is also valuable in the dynamic analysis of other kinds of the acceleration sensing systems. The relation between the frequency and the interference amplitude of the harmonic noise that the system can bear is shown in Fig. 11, and the amplitude versus the pulse width of the pulse noise in Fig. 10. In Fig. 11, ω_n represents the natural frequency, ω_i the noise frequency, a_i the interference amplitude that the threshold accelerometer can bear, and C_1, C_2 the gas film damping coefficients in different cases.

From the time responses shown in Fig. 8, we can see that the threshold accelerometer system is overdamped. In Fig. 10,

the interference amplitude of the pulse noise that the system can bear is inversely proportional to the pulse width. When the pulse width is more than 5 ms, the interference amplitude that the system can stand is close to the threshold. When the pulse width is less than 1 ms, the noise amplitude is much larger than the threshold acceleration.

In Fig. 11, the higher frequency the noise has, the stronger antijamming capability the system has. For the harmonic noise, the interference amplitudes that the system can bear are larger than the threshold, while the frequency ratio is larger than 0.03. When $\omega_i = \omega_n$, the resonance of the system occurs but the threshold accelerometer does not change the state until the noise amplitude increases to 70 g and 210 g when the damping coefficients are equal to C_1 and C_2 , respectively. The phenomenon shows that the dynamic magnification factor at $\omega_i = \omega_n$ is less than 1 when the system is overdamping, which results in the smaller resonance amplitude [24]. When $\omega_i \ll \omega_n$, the amplitude of the harmonic noise that the system can bear is less than 20 g. When $\omega_i \gg \omega_n$, the noise amplitude that the system can bear increases as the noise frequency increases. The antijamming capability of the system increases with the damping coefficient, which is in agreement with the damping analysis in [24].

V. CONCLUSION

A novel microthreshold accelerometer for an airbag restraint system is developed by utilizing the postbuckling characteristics of large deflection postbeams with both ends fixed. In the dynamic design model of the threshold accelerometer, a number of design factors such as elastic forces of postbuckling beams, damping forces calculated with the Reynolds Equations, and the tip-to-drain contact modeled by elastic Hertz theory are all taken into full consideration. The dynamic numerical simulation of the accelerometer validates the feasibility of the design method of a threshold accelerometer, with some conclusions as follows.

- 1) The accelerometer with postbuckling beams has an obvious threshold characteristic, and the nonlinear stiffness of the postbuckling beam derived above ensures the accelerometer to convert states under the triggering of threshold acceleration signal.
- 2) The thickness of the gas film between the inertial mass and the shell of the accelerometer can be regulated to improve the contact stability and the performance of resisting disturbance. After initially contacting the substrate, the accelerometer undergoes a few bounces which last a very short time until permanent contact is maintained when the damping coefficient is small.
- 3) The threshold accelerometer has a strong capacity of distinguishing signals. It cuts off automatically when the acceleration is less than a certain value.
- 4) The mechanical threshold accelerometer designed in this paper can prevent disturbances like electromagnetic and vibration noises, and improve the accuracy of the airbag restraint system.

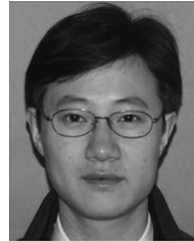
Considering the effects of the damping force and the contact force, the strong nonlinear dynamic model subjected to multi-forces is established, which is significant in the dynamic design and analysis of other kinds of acceleration sensing devices.

ACKNOWLEDGMENT

The authors gratefully acknowledge Prof. Z. Li who helped us to improve the presentation and quality of this paper.

REFERENCES

- [1] D. L. Wilcox and L. L. Howell, "Fully compliant tensural bistable micromechanisms (FTBM)," *J. Microelectromech. Syst.*, vol. 14, no. 6, pp. 1223–1235, 2005.
- [2] E. T. Enikov, S. S. Kedar, and K. V. Lazarov, "Analytical model for analysis and design of V-shaped thermal microactuators," *J. Microelectromech. Syst.*, vol. 14, no. 4, pp. 788–798, 2005.
- [3] J. Tsay, L. Q. Su, and C. K. Sung, "Design of a linear micro-feeding system featuring bistable mechanisms," *J. Micromech. Microeng.*, vol. 15, no. 1, pp. 63–70, 2005.
- [4] H. H. Hwang, Y. S. Shim, and J. H. Lee, "Modeling and experimental characterization of the chevron-type bi-stable microactuator," *J. Micromech. Microeng.*, vol. 13, no. 6, pp. 948–954, 2003.
- [5] R. A. M. Receveur, C. Marxer, F. Dupont, R. Woering, V. Larik, and N. F. Rooij, "Laterally moving bi-stable MEMS DC-switch for biomedical applications," in *Proc. 17th IEEE Int. Conf., MEMS*, Maastricht, The Netherlands, 2004, pp. 854–856.
- [6] M. Freudenreich, U. Mescheder, and G. Somogyi, "Simulation and realization of a novel micromechanical bi-stable switch," *Sens. Actuators A, Phys.*, vol. 114, no. 2, pp. 451–459, 2004.
- [7] J. S. Go, Y.-H. Cho, and B. M. Kwak, "Snapping microswitches with adjustable acceleration threshold," *Sens. Actuators A, Phys.*, vol. 54, no. 1, pp. 579–583, 1996.
- [8] T. Matsunaga and M. Esashi, "Acceleration switch with extended holding time using squeeze film effect for side airbag systems," *Sens. Actuators A, Phys.*, vol. 100, no. 1, pp. 10–17, 2002.
- [9] S. Michaelis, H.-J. Timme, M. Wycisk, and J. Binder, "Acceleration threshold switches from additive electroplating MEMS process," *Sens. Actuators A, Phys.*, vol. 85, no. 1, pp. 418–423, 2000.
- [10] M. Wycisk, J. Binder, S. Michaelis, and H.-J. Timmer, "New sensor on-chip technology for micromechanical acceleration-threshold switches," in *Proc. SPIE Conf. Electron. Structures MEMS*, Queensland, Australia, 1999, pp. 112–120.
- [11] A. Selvakumar, N. Yazdi, and K. Najafi, "Low power, wide range threshold acceleration sensing system," in *Proc. IEEE Workshop on Micro-Electro-Mechanical Syst.*, San Diego, CA, Feb. 1996, pp. 186–191.
- [12] M. Sulfridge, T. Saif, N. Miller, and M. Meinhart, "Nonlinear dynamic study of a bistable MEMS: Model and experiments," *J. Microelectromech. Syst.*, vol. 13, no. 5, pp. 725–731, 2004.
- [13] Y. B. Gianchandani and K. Najafi, "Bent-beam strain sensors," *J. Microelectromech. Syst.*, vol. 5, no. 1, pp. 52–58, 1996.
- [14] L. Que, J. S. Park, and Y. B. Gianchandani, "Bent-beam electrothermal actuators—Part I: Single beam and cascaded devices," *J. Microelectromech. Syst.*, vol. 10, no. 2, pp. 247–253, 2001.
- [15] M. Bao, *Micromechanical Transducers: Pressure Sensors, Accelerometers and Gyroscopes*. New York: Elsevier, 2000, pp. 10–25.
- [16] M. G.-E. Hak, *The MEMS Handbook*. Boca Raton, Florida: CRC, 2001, pp. 7.2–7.4.
- [17] K.-M. Chang, S.-C. Lee, and S.-H. Li, "Squeeze film damping effect on a MEMS torsion mirror," *J. Micromech. Microeng.*, vol. 12, no. 5, pp. 556–561, 2002.
- [18] C. Haixia and W. J. Kang, "Stability analysis of coupled system of magnetic head and ultra-thin gas film," *J. Hydrodynamics*, vol. 17, no. 2, pp. 134–140, 2005.
- [19] S. P. Timoshenko and J. N. Goodier, *Theory of Elasticity*, 3rd ed. New York: McGraw-Hill, 1970, pp. 89–495.
- [20] B. L. Pruitt, W. T. Park, and T. W. Kenny, "Measurement system for low force and small displacement contacts," *J. Microelectromech. Syst.*, vol. 13, no. 2, pp. 220–229, 2004.
- [21] S. Hannoe and H. Hosaka, "Electrical characteristics of micro mechanical contacts," *Microsyst. Technol.*, vol. 3, no. 11, pp. 31–35, 1996.
- [22] D. Hyman and M. Mehregany, "Contact physics of gold microcontacts for MEMS switches," *IEEE Trans. Compon. Packag. Technol.*, vol. 22, no. 3, pp. 357–362, 1999.
- [23] N. R. Aukland, H. C. Hardee, S. Hessefort, and J. P. Miller, "Contact resistance changes of silver, silver alloys, and gold plated silver coupons exposed to ozone," *IEEE Trans. Compon. Packag. Technol.*, vol. 23, no. 2, pp. 317–322, 2000.
- [24] R. W. Clough and J. Penzien, *Dynamics of Structures*. New York: McGraw-Hill, 1975.



Jian Zhao was born in Shijiazhuang, Hebei Province, China, in 1980. He received the B.S. degree in mechanical engineering from the Guilin University of Electronic Technology, Guangxi, China, in 2003, the M.S. degree in mechatronics and inertial sensors from Xidian University, Xi'an, China, in 2006. He is currently working towards the Ph.D. degree at the College of Electro-Mechanical Science, Xidian University.

His research interests include analysis of intelligent structures, design method and implementation of inertial microsensors and integration systems.



Jianyuan Jia received the B.Eng. and M.Eng. degrees in mechanical engineering from Xidian University, Xi'an, China, in 1978 and 1981, respectively.

He joined Xidian University, in 1978, where he is currently a Professor and Head of the College of Electro-Mechanical Engineering, Xidian University. He has over 80 publications on MEMS and electromechanics. His research interests range from mechatronics, CAD/CAE, engineering structural optimization on design, microsensors, microfluidics, and microscale heat transfer theory based on MEMS.



Hongxi Wang was born in Changchun, Jilin Province, China, in 1969. He received the B.E. degree in oil drilling engineering from the Daqing Petroleum Institute, Daqing, China, in 1994, the M.E. degree from Xi'an Shiyou University, Xi'an, China, in 1997, and the Ph.D. degree in mechanical design and manufacture and automation from Xidian University, Xi'an, in 2006.

He was a Senior Engineer with the China National Petroleum Corporation from 1997 to 2002. He is now an Assistant Professor at Xi'an Technological University.

His research interests include all aspects of design, fabrication, and packaging of inertial sensors and actuators.



Wanli Li received the M.S. degree in foreign languages and applied linguistics from Xidian University, Xi'an, China, in 2005.

She is a Lecturer at the Xi'an Science and Technology University. As a Part-Time Interpreter, she has translated several articles on science and technology. Her research interests include analysis and application of smart structures and scientific and technological translation.